To be published in Journal of the Optical Society of America B:

Title:	Third-order Nonlinear Optical Properties of Metallodielectric Stacks
Authors:	Nkorni Katte, Joseph Haus, Peter Powers, Andrew Sarangan, Jian Gao, and Michael Scalora
Accepted:	7 July 2011
Posted:	8 July 2011
Doc. ID:	145088

Report Documentation Page

Form Approved
OMB No. 0704-0188

1. REPORT DATE	2. REPORT TYPE	3. DATES COVERED
JUL 2011		**00-00-2011 to 00-00-2011**

4. TITLE AND SUBTITLE	5a. CONTRACT NUMBER
Third-order Nonlinear Optical Properties of Metallodielectric Stacks	5b. GRANT NUMBER
	5c. PROGRAM ELEMENT NUMBER
6. AUTHOR(S)	5d. PROJECT NUMBER
	5e. TASK NUMBER
	5f. WORK UNIT NUMBER
7. PERFORMING ORGANIZATION NAME(S) AND ADDRESS(ES) **University of Dayton,Electro-Optics Program,300 College Park,Dayton,OH,45469**	8. PERFORMING ORGANIZATION REPORT NUMBER
9. SPONSORING/MONITORING AGENCY NAME(S) AND ADDRESS(ES)	10. SPONSOR/MONITOR'S ACRONYM(S)
	11. SPONSOR/MONITOR'S REPORT NUMBER(S)

12. DISTRIBUTION/AVAILABILITY STATEMENT
Approved for public release; distribution unlimited

13. SUPPLEMENTARY NOTES

14. ABSTRACT

We report simulations of nonlinear optical transmission of an optical beam through heterogeneous metallodielectric stacks (MDSs) under the action of nonlinear absorption. We use finite element Method (FEM) with two-dimensional transverse effects and transfer matrix method (TMM) simulation techniques as complementary methods to validate the FEM approach. We find a significant nonlinear absorption effect across spectral regimes where transmission is high. We compare results with energy and group velocity results, but the enhancement of the nonlinear response is attributed to field confinement in the metal layers.

15. SUBJECT TERMS

16. SECURITY CLASSIFICATION OF:			17. LIMITATION OF ABSTRACT	18. NUMBER OF PAGES	19a. NAME OF RESPONSIBLE PERSON
a. REPORT	b. ABSTRACT	c. THIS PAGE			
unclassified	**unclassified**	**unclassified**	**Same as Report (SAR)**	**30**	

Third-order Nonlinear Optical Properties of Metallodielectric Stacks

Nkorni Katte[1], Joseph W. Haus[1,2], Peter Powers[1,2], Andrew Sarangan[1], Jian Gao[1] and Michael Scalora[3]

[1]Electro-Optics Program, University of Dayton, 300 College Park, Dayton, OH 45469, USA;

[2]Physics Department, University of Dayton, 300 College Park, Dayton, OH 45469, USA;

[3]U.S. Army Aviation and Missile Command, Charles M. Bowden Research Facility, Bldg.7804, Redstone Arsenal AL 35898-5000

Abstract

We report simulations of nonlinear optical transmission of an optical beam through heterogeneous metallodielectric stacks (MDSs) under the action of nonlinear absorption. We use finite element Method (FEM) with two-dimensional transverse effects and transfer matrix method (TMM) simulation techniques as complementary methods to validate the FEM approach. We find a significant nonlinear absorption effect across spectral regimes where transmission is high. We compare results with energy and group velocity results, but the enhancement of the nonlinear response is attributed to field confinement in the metal layers.

OCIS codes: 190.4420 Nonlinear optics, transverse effects in; 190.3270 Kerr effect.

1. Introduction

Nonlinear optical properties of heterogeneous materials with embedded metal nanoparticles have been the subject of many experimental investigations extending over the past quarter century [1-5]. Examination of different materials using degenerate four-wave mixing (DFWM) techniques has turned up surprisingly large optical nonlinear responses for metal nanoparticles and revealed differing dominant mechanisms for the nonlinear optical behavior based on materials, particles size and shape, and excitation wavelength. Effective nonlinear optical properties of ellipsoidal particle shapes and core/shell particles have been explored, as well [5, 6].

Only the magnitude of the third-order nonlinearity can be obtained from DFWM experiments. However, applying the Z-scan technique both real and imaginary third-order contributions are extracted from the data [7, 8, 9]. Nonlinear optical properties of materials have been widely studied with the Z-scan technique for many different applications. As developed by Sheik-Bahae et al [7] a (Gaussian) laser beam is focused in free space; a sample is positioned along the propagation (Z) axis of the laser beam while measuring the irradiance on a detector in the far field. In a sample with a linear optical response no transmission change is expected; however, in a sample with a nonlinear response the beam has a focus or defocus (refractive) effect due to the real part of the nonlinearity and an amplitude effect due to its imaginary part. By analyzing the irradiance profile the Z-scan technique provides valuable knowledge about the sample's effective nonlinear coefficients.

In this paper we use numerical techniques to examine the nonlinear transmission characteristics of multi-layer thin film materials that are not described by one effective index

parameter because of important interference effects. One film layer is a metal and the other layer is a dielectric; the heterogeneous material is called a metallodielectric stack (MDS). Experimental investigations reported significant nonlinear response of MDSs with constituent metal films of silver (Ag), gold (Au) or copper (Cu) [10-13]. Nevertheless there is a need to investigate these materials with more efficient and accurate numerical techniques in order to account for the underlying physical processes observed in experiments. The nonlinear response of MDS samples were studied with copper films and a large effect was produced [13, 14].

We apply a Finite Element Method (FEM) with radial symmetry to numerically solve for the Z-scan experiment of a MDS. Our model solves the corresponding nonlinear Maxwell's equation; the amplitude and the phase of the electromagnetic field at the exit interface of the MDS are used for transforming to the far-field regime. The standard Z- scan technique which has been used extensively to characterize several kinds of materials including a 1D photonic band gap device, such as our MD stack, usually ignores the losses due to internal multi-interference and back reflections, which contributes to the absorption within each layer [9]. Even when these phenomena are considered in the case of a bidirectional beam propagation method, transverse effects important in describing the beam profile are often approximately handled. Meng [15] and Chen [16] studied the nonlinear response of photonic band gap structures with plane wave or one transverse dimension using the finite difference-time domain (FDTD) method. This method is both memory and computation cycle intensive.

Inclusion of transverse effects in the simulations is necessary to capture the nonlinear refractive effects from Z-scan experiments. Even those who have included significant nonlinearity within some of the layers of the 1D photonic band gap stack in their model chose to address the nonlinear phase shift by assuming locally a plane wave is incident [16]. In the FEM

approach we treat a Gaussian input beam and define the physics of the problem to include back reflections, diffraction and multi-interference throughout the thin layers of material.

2. Numerical Approaches

We apply two approaches to studying the properties of our MDSs: The transfer matrix method and the finite element method. For linear systems we find them to be complementary techniques for understanding the physics of our systems and validate the FEM simulations.. In the past we have used them for studying super-resolution in MDSs [17, 18]. The linear complex refractive indices of the metals (Cu, Ag) used in our simulations are taken from [19], while the values for the dielectrics (TiO_2 and ZnS) are measured values obtained at the University of Dayton Nanofabrication Laboratory. Ellipsometric measurements of the optical constants of sputtered Ag layers (>15nm) agrees with published results [14].

To illustrate our computational approach two different MDS designs are reported in this paper. The first structure, denoted as MDS1, is made of films with TiO_2 and Cu and the second one, called MDS2, is made with ZnS and Ag films. The MDS1 sample in this paper has a total of 9 layers with material and layer thickness as follows: TiO_2 (40nm)/[Cu(20nm)/TiO_2(80nm)] $_{3.5}$/TiO_2(40nm). The sample has a total of 80 nm of Cu metal and is 400 nm thick; the subscript 3.5 on the square brackets indicated that the second layer is missing from the fourth period. The MDS2 sample has seven alternating layers of ZnS and Ag in the following sequence: ZnS (40nm)/ [Ag (20nm)/ ZnS (80nm)] $_{2.5}$ ZnS (40nm). The Cu metal was chosen because it is reported to have a high third-order nonlinear coefficient among the metals of interest [4-6, 10-13]. Silver has been the subject of many experimental studies. Although in comparison to Cu, it is reported to have third-order nonlinearity is relatively small [5].

2.1 Transfer Matrix Method

We applied the transfer matrix method (TMM) to study the linear properties of the field for different angles of incidence and to determine the dispersion characteristics like the group and energy velocity indexes. In the linear regime the TMM is also used to verify that the FEM results accurately represent the physical problem. Using the TMM method the field is decomposed into plane waves and the forward- and backward-propagating amplitudes are found by using a series of 2x2 matrices that contain the optical path lengths in the adjacent media and the polarization-dependent boundary conditions [20]. For linear media the TMM is a faithful representation of the field across the sample. The properties that are most often examined are the transmittance and reflectivity of the sample. The transmittance and reflectance amplitudes are expressed in complex form as

$$t = |t| e^{i\phi_t}, \quad r = |r| e^{i\phi_r}. \tag{1}$$

The quantities ϕ_t and ϕ_r are the phase changes in the transmitted and reflected wave amplitude due the complex interference between the different wave paths. The plane-wave transmittance and reflectance coefficients are defined for any angle of incidence as

$$T = \frac{n_t \cos\theta_t}{n_0 \cos\theta_i} |t|^2, \quad R = |r|^2; \tag{2}$$

θ_i and θ_t are the incident and transmitted angles of incidence, and n_0 and n_t are the incident and transmitted medium refractive indices, resp. The absorbance, A, is calculated using the relation

$$A = 1 - T - R \quad . \tag{3}$$

The phases in Eq. (1) contain information about spectral dispersion of the transmitted and reflected waves [21]. The phase of the transmitted wave is related to an effective propagation constant used for optical interactions

$$\phi_t = k_e L \quad , \tag{4}$$

where L is t he thickness of the sample and k_e is the effective propagation constant. A quantity of interest in the present studies is the group velocity index, which is defined as:

$$N_g = c\frac{\partial k_e}{\partial \omega} = \frac{c}{L}\frac{\partial \phi_t}{\partial \omega} \quad . \tag{5}$$

The energy velocity in a dispersive medium is distinct from the group velocity and can be compared with the group velocity [22]. The definition of the energy velocity is based on the energy density

$$U = \frac{1}{4}\left(\frac{\partial(\omega\varepsilon)}{\partial\omega}|E|^2 + \frac{\partial(\omega\mu)}{\partial\omega}|H|^2\right) = U_E + U_M \quad ; \tag{6}$$

and the Poynting vector:

$$\mathbf{S_{av}} = \frac{1}{2}\mathbf{Re(E\times H^*)} \quad . \tag{7}$$

The average energy velocity is defined as a ratio of the integral across the sample for these two quantities:

$$V_E = \frac{\int_0^L \mathbf{S}_{av} \cdot \mathbf{dz}}{\int_0^L U dz} \quad . \tag{8}$$

Analogous to the group velocity index the energy velocity index is defined as

$$N_E = c / V_E \quad . \tag{9}$$

The transmittance, absorbance and the energy and group indexes for these two designs are plotted in Figures 1 and 2 as a function of wavelength. The group and energy indexes both have relatively high values across the transparency regime and by both measures the light slows down further at the transmission edges. The group indexes for both samples have similar characteristics both are relatively flat values across the transparency regime, peak at the edges and then fall off. The group index has a pronounced peak at the edges of the transmission spectral bands, which approaches or exceeds 20 for these portions of the transmission band. The energy velocity indexes on the other hand indicate slower light outside the transmission bands, where the signal is feeble. From the transmittance, absorbance and index results in Figure 1 a wide transmission spectral band is observed extending from below 500 nm to greater than 800 nm.

The spectral width of the transmission bands is determined by the properties of the materials, the thickness of the films and the number of layers. In our transparent metal designs the first and last layers are dielectric films that are half as thick as the bulk dielectric layers. This has the affect of raising the transmittance and reducing the local Fabry-Perot-like peaks in the spectrum [23].

The indexes do not directly reveal whether or not the field is localized in the metal films. At the long-wavelength, pass-band edge there is a peak in the absorbance that corresponds to the group index peak; the absorbance is an indication of the field's localization in the metal film. However, the short wavelength pass band either does not have an absorbance peak or the absorbance peak does not coincide with the local maximum of the group index. We find that the field near these wavelengths is largely localized in the dielectric and we attribute the slow group velocity to a coupled Fabry-Perot cavity effect.

2.2 Finite Element Method

The open aperture Z-scan experiment reveals the effect of the two photon absorption on the transmission. The FEM used in this calculation is implemented using COMSOL 3.5a. The FEM method was also used to determine the closed aperture Z-scan transmissivity. The corresponding nonlinear wave equation which is solved by FEM in cylindrical coordinates, when the input beam of wavelength λ is TE polarized and the free space wavenumber is $k_0 = 2\pi/\lambda$. The wave propagates in the z direction is given below

$$\nabla \times \left(\frac{1}{\mu_r} \nabla \times \mathbf{E}_\varphi \right) - \varepsilon_r k_0^2 \mathbf{E}_\varphi = 0. \tag{10}$$

The relative magnetic permeability μ_r is unity for all the materials used in our calculations. The dielectric function depends on the irradiance with the following dependence:

$$\varepsilon_r = \left(n_L + \gamma \mathbf{S}_{\mathbf{av},z} \right)^2, \tag{11}$$

where n_L is complex the refractive index of the metal or the dielectric in the linear regime, and the nonlinear coefficient, $\gamma = n_2 - \frac{i\lambda\beta_2}{4\pi}$, has a complex value. The longitudinal component of the Poynting vector was used in Eq. (11). The Kerr coefficient, n_2, affects the refractive index and the two-photon absorption coefficient, β_2, produces a nonlinear absorption effect. The effect on the phase and log-amplitude is proportional to the irradiance profile. In our calculations we take advantage of the cylindrical symmetry of the beam. The vector field is given by $\mathbf{E}_\varphi = \hat{e}_\varphi E$ where the unit vector is transverse to the direction of propagation. The beam width at the focal plane is w_0 and The Rayleigh range $z_0 = \pi w_0^2 / \lambda$ .The beam width at position z is $w(z) = w_0\sqrt{1+\left[\frac{z}{z_0}\right]^2}$. The radius of curvature of the phase is $R(z) = z\left[1+\frac{z_0^2}{z^2}\right]$. The scalar field is given by Eq. (8) below.

$$E(Z,r,t) = E_0 \frac{w_0}{w(z)} \exp\left(-\frac{r^2}{w^2(Z)} + i\frac{\pi r^2}{\lambda R(z)} + i\phi\right) \quad . \tag{12}$$

The linear optical transmission and absorption characteristics of MDS1 using TMM are plotted in Figure 1. The FEM transmission spectrum was calculated for specific wavelengths and was in close agreement with the TMM results.

The field inside the sample was calculated by both the TMM and FEM methods. Figure 3a presents the TMM calculated field amplitude throughout the MDS1 sample at a wavelength of 650 nm for three angles of incidence. The wavelength was chosen because it is near the transmittance maximum. TMM results on the left shows the S-polarized field dependence inside the sample for several angles of incidence. We note that the field localization inside the metal

has the largest amplitude for normal incidence. Normal incidence should have a large nonlinear effect in the sample. On the right is a comparison of the fields at normal incidence in the sample found between the FEM and the TMM simulations. The two results are nearly identical and provide a direct validation of the FEM approach for this case.

To validate the FEM simulations for the nonlinear transmission characteristics a Z-scan experiment of a homogeneous material was simulated. An illustration of the transmission results for a Z-scan experiment is shown in Figure 4a. The sample is moved a distance z from the focus of a Gaussian beam, as illustrated in Figure 4b. The Rayleigh range, $z_0=kw_0^2/2$, is used to scale the position of the sample relation to the beam's focal plane. The beam waist at the focal plane is w_0. In the far field an aperture is placed in front of the detector and the irradiance is recorded as a function of z. In a linear medium the transmittance is constant. On the left in Figure 4 are the results of our simulations for a L=400 nm thick sample with Kerr nonlinearity $n_2= 9x10^{-12}$ cm^2/W. The refractive index of the sample was chosen as 1.2 and the laser wavelength is 532 nm. The material parameters are not specific to any realistic material, but have been chosen to compare with analytic results. The Gaussian beam waist is $w_0 = 20$ microns and the peak irradiance at the focal plane is 11.93 GW/cm^2. A CW beam is used in the simulations. The transmittance as function of position z for the Z-scan experiment is given by Eq. (9) below. Where E_{NL} and E_L are the nonlinear electric field and linear electric fields respectively at aperture which is determined by a Fourier transform of the electric field at the exit layer of the sample, and r_d is the radius of the aperture in front of the detector. The transmission is calculated from the relation:

$$T(z) = \left[\frac{\int_0^{r_d} r dr \left| E_{NL}(z,r) \right|^2}{\int_0^{r_d} r dr \left| E_L(z,r) \right|^2} \right]. \tag{13}$$

The numerical Z-scan results are compared with the analytical results derived for a thin nonlinear medium [7]. The equation for the analytical result is:

$$T_r = 1 + \left(\frac{4Z\Phi}{(Z^2+9)(Z^2+1)} \right) \tag{14}$$

where $Z=z/z_0$ and $\Phi = k_0 n_2 L I$, where I is the irradiance, L is the sample thickness, and k_0 is the free space wavenumber. The transmittance is normalized to unity in the linear regime. The position and size of the peaks from the FEM simulations are in close agreement with the analytical results. The steeper drop of the FEM curves is attributed to non-perturbative nonlinear effects in the simulation.

Next we consider the propagation of a typical CW Gaussian beam through the MDS samples. The complex field at the exit layer of the stack is used to calculate the normalized transmittance according to Eq. (13). We assume a CW source; with COMSOL we extract the phase and the amplitude of the Electric field at the exit layer of MDS, which is numerically integrated by taking a Bessel transform to determine the electromagnetic field at the far field.

The FEM Z-scan trace determines the overall nonlinear optical response of the samples. We obtain the nonlinear optical constant of the materials used in the simulations. As a check of the nonlinear FEM calculations both FEM and TMM results are compared for the linear case and

check agreement before solving the nonlinear problem. The results are presented for two MDS samples. First we consider the sample composed of Cu and TiO_2 layers (MDS1) and then we study the sample made from Ag and ZnS layers (MDS2).

The origin of the nonlinearity in our simulations is attributed to electronic transitions, which are represented by a third-order susceptibility coefficient. Classical electromagnetic local field enhancements caused by electron oscillations known as surface plasmons will amplify the nonlinear effect. Additional nonlinear effects have been identified, such as, intraband and interband transitions which affect the susceptibility when electrons electrons fill empty states. A Fermi smearing effect, commonly known as the hot electron contribution, creates a sea of thermally excited electrons with energy levels around the Fermi energy. These effects were recently examined for Ag films by Owens et al. [10, 11]. The electron temperature changes under strong fluence irradiation are large enough to elicit strong transmittance changes.

3. Z-scan Results

The group and energy indexes are included to study wavelength regions for slow light within the material; as a first guess the slow light regions may be expected to show an enhanced of the nonlinear optical response and the results could be correlated with our simulations.

For MDS1 we chose refractive and absorptive third-order nonlinear parameters for Cu as: $n_2 = 5\times10^{-11} cm^2/W$ and $\beta_2 = 5\times10^{-6} cm/W$ similar to the results published in [24]. However, in experiments these values will depend on wavelength; we simplify the problem by assuming constant nonlinear parameters for all wavelengths. The nonlinear parameters for TiO_2 are $n_2 = 1.33\times10^{-16} cm^2/W$ and $\beta_2 = 13\times10^{-9} cm/W$ [25]. The normal incident, on-axis electric

field amplitudes for five wavelengths across the transmission band are shown in Figure 5. The four regions delineated by vertical lines are the Cu metal films. The field profile at 820 nm has the strongest amplitude in the first two metal films and the one at 500 nm penetrates the least. These are both wavelengths where the group index has a peak and the energy index is high, but the absorbance peak only coincides with the long wavelength group index maximum. The metal nonlinearity produces its strongest affect in this sample at the long wavelength peak.

The numerical results for the open aperture Z-scan MDS1 simulation are shown in Figure 6. In this case the irradiance was constant and at the focal plane it is 1.9 GW/cm^2. The linear transmittance in each case has been normalized to unity. The strongest relative change around 15 % in the transmittance is at 650 nm, where the penetration of the electric field in the metal films is strong. A strong dip of about 8 % is observed at 820 nm and its linear transmittance is about five times lower than at 650 nm. The field localization in each metal layer at 650 nm is high and coincidentally it has the largest transmittance of the cases considered in Figure 5. We do not find a correlation between slow light regimes and strong nonlinear responses.

The Electric field amplitude for the MDS2 sample is plotted in Figure 7 shows the beam's spread in both the longitudinal and transverse directions. The input radial beam shape is a Gaussian function, Eq. (8) with the sample placed at the focal plane. In this case the irradiance used is 47.74 GW/cm^2. The nonlinear parameters we use for Ag are: $n_2 = 2\times10^{-11} cm^2/W$ and $\beta_2 = 3.3\times10^{-8} cm/W$ [25]. The nonlinear refraction coefficient of ZnS is zero, while its two-photon absorption coefficient is $\beta_2 = 3.4\times10^{-9} cm/W$. These values are taken from [25] and applied to all wavelengths.

The field amplitude squared for $r=0$ are plotted in Figure 7 for five wavelengths across the transmission band. At the short wavelength peak of the group index the field is localized outside the metal films. The largest reported field localization occurs at the long wavelength peak. The field profile through the metals has a relative minimum in the metals to avoid excessive absorption losses in the structure. The field penetration for wavelengths 650 nm and 680 nm is comparable with an overall edge at the 650 nm wavelength.

The open aperture Z-scan of MDS2 is shown in Figure 8 for five different wavelengths. The irradiance at the focal plane was the same as applied in our simulations of MDS1. The weakest nonlinear effect was observed at the short wavelength edge of the transmission band. The 650 nm wavelength shows the strongest nonlinear effects and its value does not correspond to a peak in the group index or an absorption maximum. The smaller value of β_2 for Ag leads to a smaller minimum in the normalized transmittance curves. The results correlate with the field localization in the metal films. Namely, higher localization means larger nonlinear changes. The absorbance peaks, energy velocity and group velocity are no guide to the regions of greatest nonlinear responses.

4. Conclusion

Using FEM numerical simulations we studied the open aperture Z-scan results of nonlinear absorption in metallodielectrics. The localization of the field in the metal region always corresponded to a greater nonlinear effect. The group and energy indexes or absorption maximum use as an indicator of the most effective nonlinear wavelengths were not highly correlated for the cases we studied. The simulations used a FEM technique to characterize the nonlinear transmission properties of 1D metallic PBG structures with material parameters taken

from the literature. Our method incorporates the transverse beam profile, interference and diffraction effects. The accuracy of the simulations was validated using TMM techniques and analytical results. Our purely refractive nonlinear results agree very well with the Z-scan theory and we conclude that the FEM technique is a faithful model for such systems where back reflections and resonances play an important role in the linear and nonlinear processes. This method applies equally well for multi-layer stacks made from purely dielectric materials. It can be adapted to study nonlinear optical properties of higher-dimensional photonic crystals.

With the FEM tool the interesting physics of photonic crystals can be studied to include open and closed aperture Z-scan geometries. Besides potential broad-band optical limiter applications [28] metallodielectric stacks have potential for super-resolving imaging properties [17, 22, 29-30]. The FEM technique can be applied to these problems, as well, resolves the very memory intensive problem, by assuming axial symmetry scaling down the dimension of the problem from three to two.

We included the nonlinear refractive indices of the dielectric materials in our simulations; however, for the examples in this paper the two photon absorption coefficients of the metals dominated the nonlinear optical properties in these simulations. These results are a prelude to future experimental investigations of the nonlinear optical properties of MDSs. In the future we will apply realistic input beam characteristics, including pulse operation, thermal effects, and we will use experimentally derived material properties to provide a direct comparison with experimental results.

5. References

[1] D. Ricard, Ph. Roussignol and C. Flytzanis, "Surface-mediated enhancement of optical phase conjugation in metal colloids," Opt. Lett. **10**, 511-513 (1985).

[2] M. J. Bloemer, J. W. Haus and P. R. Ashley, "Degenerate four-wave mixing in colloidal gold as a function of particle size" J. Opt. Soc. Am. B **7**, 790-795 (1990).

[3] M. J. Bloemer, P. R. Ashley, J. W. Haus, N. Kalyaniwalla and C. R. Christensen, "Third-order Optical Nonlinearities in Waveguide Geometry," IEEE J. of Quantum Electron. **26**, 1075-1080 (1990).

[4] L. Yang, K. Becker, F. M. Smith, R. H. Magruder III, R. F. Haglund, Jr., Lina Yang, R. Dorsinville, R. R. Alfano, and R. A. Zuhr, "Size dependence of the third-order susceptibility of copper nanoclusters investigated by four-wave mixing," J. Opt. Soc. Am. B **11**, 457-461 (1994).

[5] R. J. Gehr and R. W. Boyd, "Optical Properties of Nanostructured Optical Materials," Chem. Mater. **8**, 1807-1819 (1996).

[6] J. W. Haus, R. Inguva and C. M. Bowden, "Effective-medium Theory of Nonlinear Ellipsoidal Composites," Phys. Rev. A **40**, 5729-5734 (1989).

[7] M. Sheik-Bahae, A. A. Said, T. Wei, D. J. Hagan, and E. W. Van Stryland, "Sensitive measurement of optical nonlinearities using a single beam," IEEE J. Quantum Electron. **26**, 760-769 (1990).

[8] R. A. Ganeev, A. I. Ryasnyanskii, M. K. Kodirov, S. R. Kamalov and T. Usmanov, "Nonlinear Optical Characteristics of Colloidal Solutions of Metals," Optics and Spectroscopy **90**, 568-573 (2001).

[9] J. Wei and M. Xiao, “A Z-scan model for Optical nonlinear nanometric films,” J. of Optics A, Pure Applied Optics **10,** 115102 (2008).

[10] D. T. Owens, C. Fuentes-Hernandez, J. M. Hales, J. W. Perry, and B. Kippelen, "Nonlinear optical properties of induced transmission filters," Opt. Express **18**, 19101-19113 (2010)

[11] D. T. Owens, C. Fuentes-Hernandez, J. M. Hales, J. W. Perry, and B. Kippelen, “A comprehensive analysis of the contributions to the nonlinear optical properties of thin Ag films,” J. Appl. Phys. **107**, 123114 (2010).

[12] T. K. Lee, A. D. Bristow, J. Hubner, J. and H. M. van Driel, “Linear and nonlinear optical properties of Au-polymer metallodielectric Bragg stacks,” J. Opt. Soc. Am. B **23**, 2142 (2006).

[13] N. N. Lepeshkin, A. Schweinsberg, G. Piredda, R. S. Bennink and R. W. Boyd, “Enhanced nonlinear optical response of one-dimensional metal-dielectric photonic crystals,” Phys. Rev. Lett. **93**, 123902 (2004).

[14] R. S. Bennink, Y. K. Yoon, R. W. Boyd and J. E. Sipe, “Accessing the optical nonlinearity of metals with metal-dielectric photonic bandgap structures,” Opt. Lett. **24**, 1416-1418 (1999).

[15] Z.-M. Meng, H.-Y. Liu, Q.-F. Dai, L.-J. Wu, Q. Guo, W. Hu, S.-H. Liu, S. Lan, and V. A. Trofimov “ Dependence of nonlinearity enhancement on power density in photonic crystals characterized by numerical *Z*-scan experiments based on the finite-difference time-domain technique,” J. Opt. Soc. Am. B **25**, 555-563 (2008).

[16] S. Chen, W. Zang, A. Schülzgen, X. Liu, J. Tian, J. V. Moloney, and N. Peyghambarian, "Modeling of Z-scan characteristics for one-dimensional nonlinear photonic bandgap materials," Opt. Lett. **34**, 3665-3667 (2009).

[17] N. Katte, J. W. Haus, J.B. Serushema, and M. Scalora "Super-resolving properties of metallodielectric stacks," COMSOL conference, Boston 2010.

[18] J.W. Haus, M. Scalora, N. Katte and J. B. Serushema, "Metallodielectrics as Metamaterials," "Proc. Of the SPIE Optics and Photonics Conference **7756,** 77560F (2010).

[19] E. D. Palik, *Handbook of Optical Constants of Solids* (Academic Press, New York, 1985).

[20] P. Yeh, *Optical waves in layered media,* Goodman, J.W. (ed.). (New York,Wiley, 1988).

[21] M. Bertolotti, C. M. Bowden and C. Sibilia (Eds), *Nanoscale Linear and Nonlinear Optics*: Intern. School on Quantum Electronics, Erice, Sicily, (AIP Conf. Proc., Vol. 560) (Melville, NY: AIP, 2001).

[22] M. Bloemer, G. D'Aguanno, N. Mattiucci, M. Scalora, and N. Akozbek, "Broadband super-resolving lens with high transparency in the visible range," Appl. Phys. Lett. **90**, 174113 (2007).

[23] G. D'Aguanno, M. Centini, M. Scalora, C. Sibilia, M. J. Bloemer, C. M. Bowden, J. W. Haus, and M. Bertolotti, "Group velocity, energy velocity, and superluminal propagation in finite photonic band-gap structures," Phys. Rev. E **63**, 036610 (2001).

[24] C. Fuentes-Hernandez, L. A. Padilha, J. M. Hales, D. Owens, J. Kim, S. Webster, J. W. Perry, D. J. Hagan, E. W. VanStryland, and B. Kippelen, "Enhanced Nonlinear Absorption in Low-Finesse Metal-Dielectric Fabry-Perot Resonators," in *Conference on Lasers and Electro-Optics/International Quantum Electronics Conference*, OSA Technical Digest (CD) (Optical Society of America, 2009), paper IThD5.

[25] C. Fuentes-Hernandez, L. A. Padilha, J. M. Hales, D. Owens, J. Kim, S. Webster, S. R. Marder, J. W. Perry, D. J. Hagan, E. W. Van Stryland, and B. Kippelen, "The Nonlinear Optical

Response of Transparent Metal-Dielectric Multilayer Structures," in *Integrated Photonics and Nanophotonics Research and Applications*, OSA Technical Digest (CD) (Optical Society of America, 2009), paper JTuA2.

[26] R. L. Sutherland, D.G. McLean and S. Kirkpatrick, "Handbook of nonlinear optics" 2nd edition, (CRC Press, 2003).

[27] C.Fuentes-Hernandez and B.Kippelen " Nonlinear Optical properties of Copper based photonic bandgap structures at the onset of interband transitions" Nonlinear Optics and Quantum Optics **40**, 69-82 (2010).

[28] M. C. Larciprete, C Sibilia, S Paoloni, M Bertolotti, F. Sarto, M. Scalora, "Accessing the optical limiting properties of metallo-dielectric photonic band gap structures," J. Appl. Phys. **93**, 5013-5017 (2003).

[29] M. Scalora, G. D'Aguanno, N. Mattiucci, M. J. Bloemer, D. de Ceglia, M. Centini, A. Mandatori, C. Sibilia, N. Akozbek, M. G. Cappeddu, M. Fowler, and J. W. Haus, "Negative refraction and sub-wavelength focusing in the visible range using transparent metallo-dielectric stacks," Opt. Express **15**, 508-523 (2007)

[30] D. de Ceglia, M. A. Vincenti, M. G. Cappeddu, M. Centini, N. Akozbek, A. D'Orazio, J. W. Haus, M. J. Bloemer and M. Scalora, "Tailoring Metallodielectric Structures for Super Resolution and Super guiding Application in the Visible and near IR Ranges," Phys. Rev. A **77**, 033848 (2008).

Figure Captions

Figure 1: Optical properties of the TiO_2 and Cu multilayer system called MDS1. The sequence is a 40 nm thick TiO_2 layer followed by three and one-half periods of 20 nm thick Cu film and 80 nm thick TiO_2 film and finally a 40 nm thick TiO_2 film at the other end. This design is a transparent metal and it is denoted by the following notation describing the thickness of each layer: $TiO_2(40nm)/[Cu(20nm)/TiO_2(80nm)]_{3.5}$ $/TiO_2(40nm)$. (a): Transmittance and absorbance versus wavelength. (b): Group and energy indexes versus wavelength.

Figure 2: Optical properties of the ZnS and Ag multilayer system called MDS2. The sequence of layers using the same notation given in figure 1 is ZnS (40nm)/[Ag(20nm)/ZnS(80nm)] $_{2.5}$ZnS(40nm). (a): Transmittance and absorbance versus wavelength. (b): Group and energy indexes versus wavelength.

Figure 3: Shows field squared at a wavelength of 650nm throughout the MDS1 sample. The vertical lines are positions of the metal/dielectric interfaces. (a) TMM plot of field squared for TE polarization at different incident angles (0 degrees (solid), 30 degrees (long dash) and 45 degrees (dotted)). (b) FEM and TMM plot of the field at plane wave normal incidence.

Figure 4: (a): Z-scan for a 400nm thick material whose refractive index at 532nm is 1.2 and has a nonlinear refractive index $n_2= 9x10^{-16}m^2/W$. (b): Z-scan setup. The sample is moved a distance z from the beam focus while recording the transmittance at a detector placed behind a closed (i.e. small) or open aperture in the far field regime.

Figure 5: The electric field amplitude squared versus position in the sample MDS1. The vertical lines mark the interfaces between the TiO_2 and Cu films.

Figure 6: Open Aperture Z-scan Curves for MDS1. The position of the sample is normalized by the Rayleigh range, z_0.

Figure 7: The electric field amplitude squared versus position in the sample MDS2. The vertical lines mark the interfaces between the ZnS and Ag films.

Figure 8: Open Aperture Z-scan Curves for MDS2. The position of the sample is normalized by the Rayleigh range, z_0.

Figure 1 Katte et al.

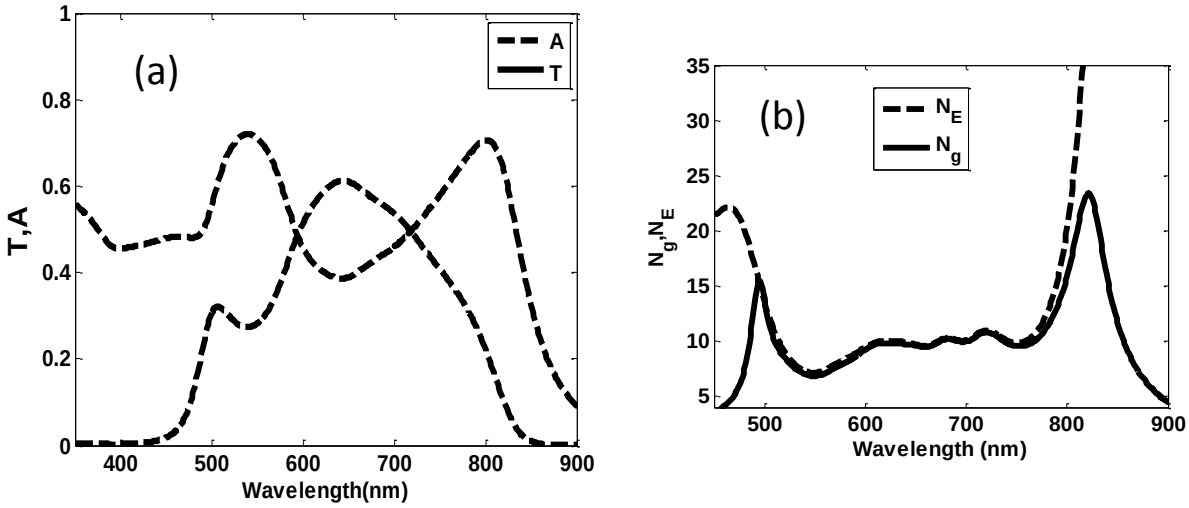

Figure 2 Katte et al.

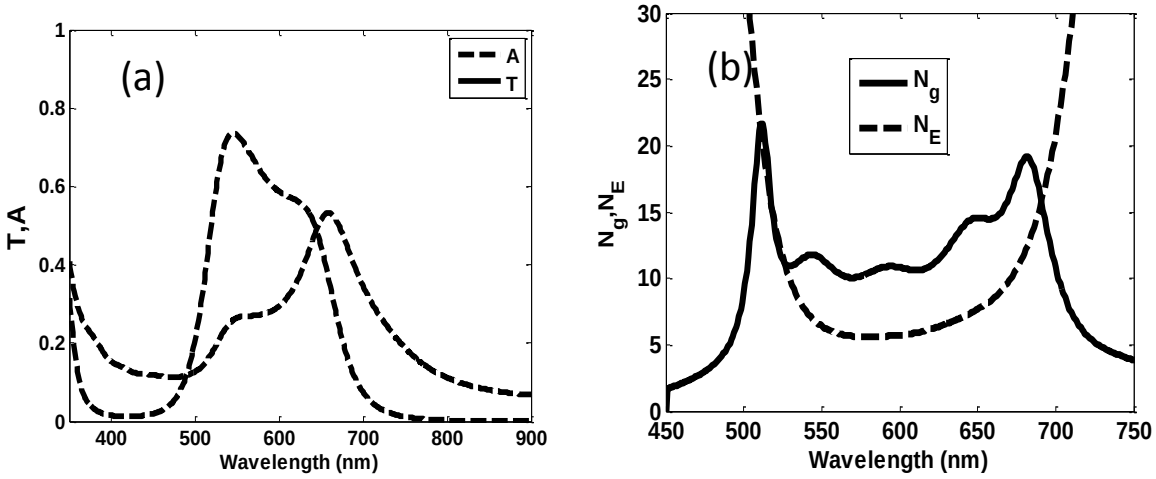

Figure 3 Katte et al.

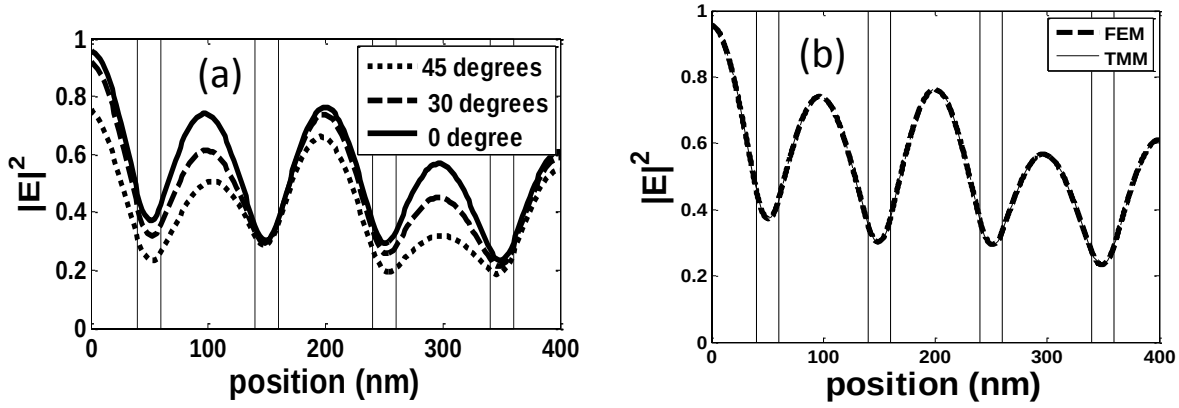

Figure 4 Katte et al.

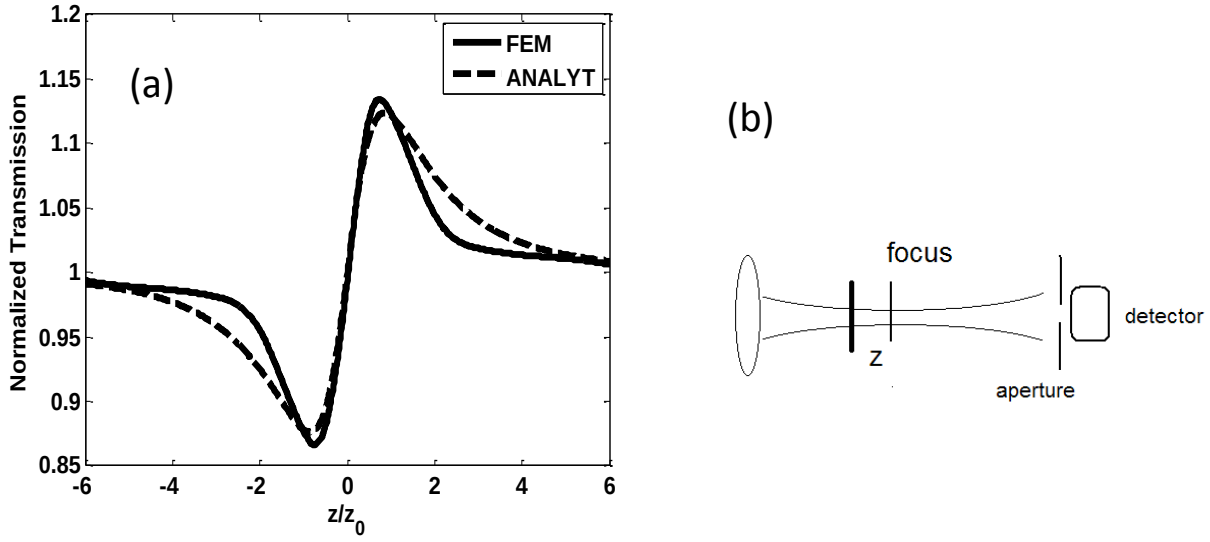

Figure 5 Katte et al.

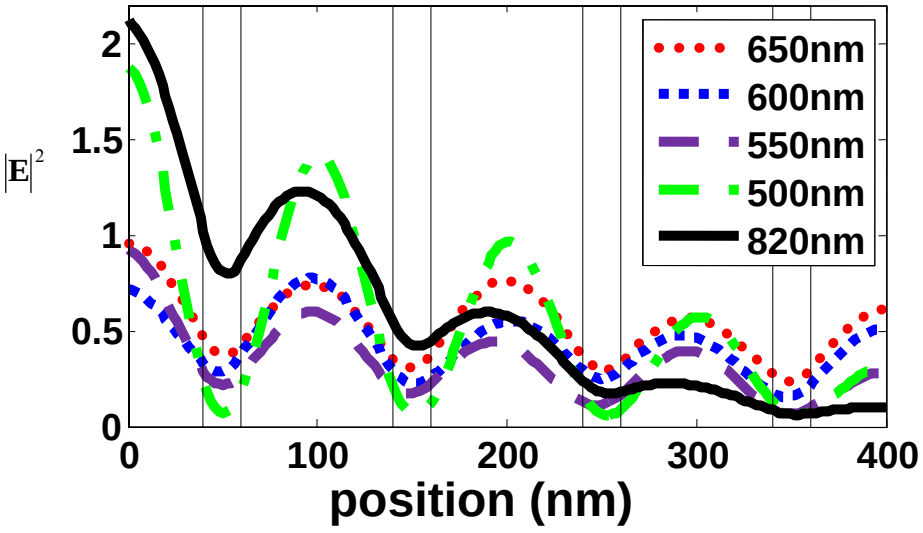

Figure 6 Katte et al

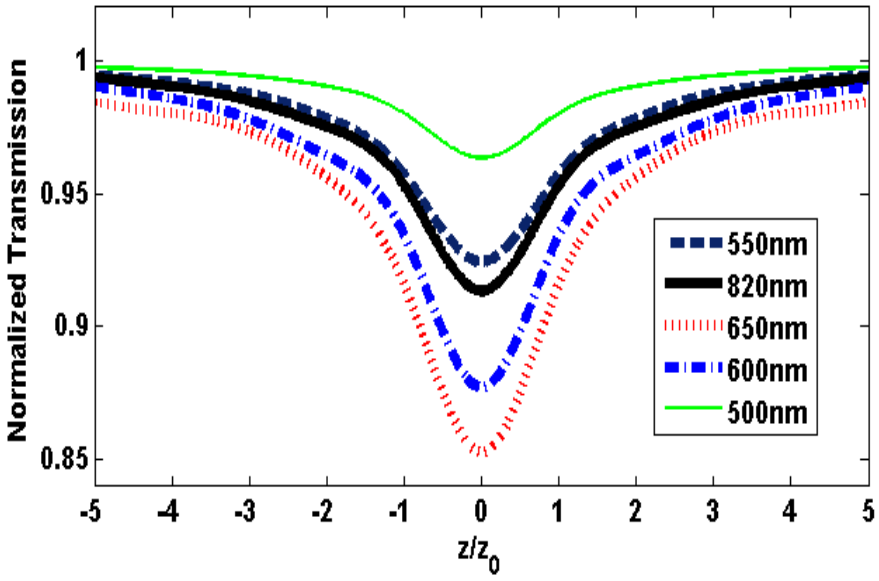

Figure 7 Katte et al.

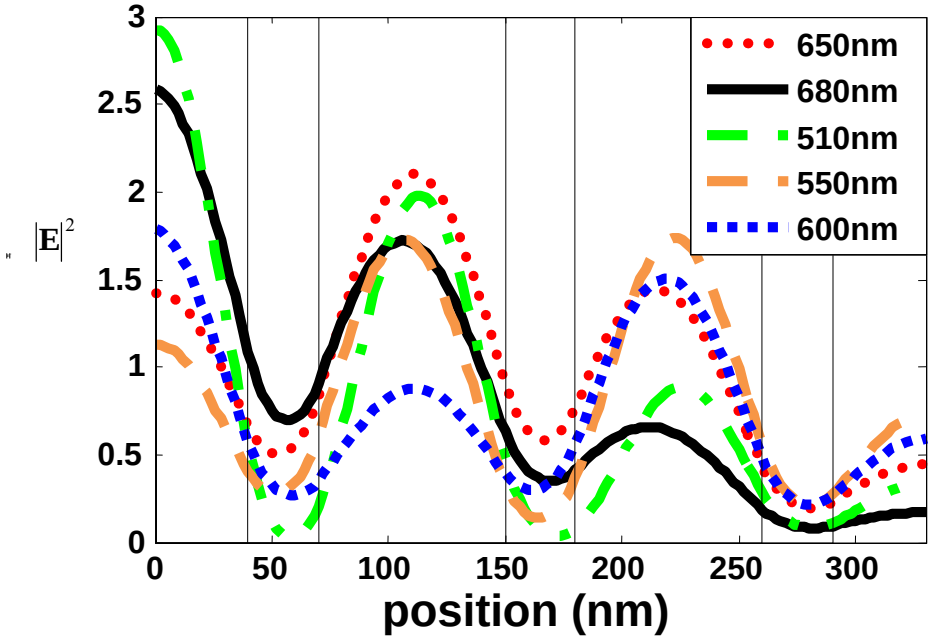

Figure 8 Katte et al.